Research Article Vol. 33, No. 8 / 21 Apr 2025 / Optics Express 16976
Optics EXPRESS

Enhanced optical properties of translucent YVO_4 ceramic fabricated by spark-plasma-sintering (SPS) via texture-controlled microstructure

LIHONG LIU,[1] JIGUANG LI,[2] KOJI MORITA,[2] BYUNG-NAM KIM,[2] AND TOHRU S. SUZUKI[1,*]

[1] *Optical Ceramics Group, Research Center for Electronic and Optical Materials, National Institute for Materials Science, Tsukuba, Ibaraki 305-0047, Japan*
[2] *Polycrystalline Optical Material Group, Research Center for Electronic and Optical Materials, National Institute for Materials Science, Tsukuba, Ibaraki 305-0047, Japan*
[*] *Suzuki.tohru@nims.go.jp*

Abstract: Achieving an (001) orientation-aligned structure in the YVO_4 green bodies by colloidal processing with a strong magnetic field can enhance the optical properties of translucent YVO_4 ceramics fabricated by a spark-plasma-sintering (SPS) technique. YVO_4 green bodies with orientation along the (001) direction are successfully attained from a well-dispersed and highly stable YVO_4 slurry containing 15 vol% YVO_4 nanopowders prepared at 1 wt% of dispersant under a pH > 9. By designing the (001) texture of YVO_4 with aligning the slip casting direction parallel to the magnetic field B during the slip casting, the YVO_4 SPSed at a temperature of $T = 1300$ °C gained much higher transmittance than that of non-textured random YVO_4, indicating that controlling the microstructure by colloidal processing with a strong magnetic field is an effective approach to improving the optical properties of YVO_4 ceramics.

1. Introduction

Yttrium-orthovanadate (YVO_4), which crystallizes in a tetragonal structure and belongs to a space group D_4 h, is a highly versatile crystalline material widely used in diverse fields such as polarization optics [1], phosphors [2], and laser host material [3]. In solid-state laser application, YVO_4 is a very known transparent host material for the rare earth ions, such as Nd^{3+}, for developing micro-chip lasers with laser diode pumping due to its high absorption coefficient, high optical transparency in the 400-5000 nm range, large emission cross section. These properties allow YVO_4:Nd to achieve high optical efficiency even at small size, [4] which has driven interest in developing larger-sized YVO_4:Nd crystals to support high-power, high-efficiency laser designs. However, the traditional single-crystal growth method for producing high quality and large-sized crystals is costly, and the process is complex and difficult to control. As an alternative approach, the fabrication of transparent YVO_4:Nd laser ceramics offers a promising route to producing large-sized YVO_4:Nd materials. Previously, YVO_4:Nd was considered unsuitable for high-power operation because its thermal conductivity was thought to be only half that of $Y_3Al_5O_{12}$:Nd (YAG:Nd) [5], and it was believed that highly Nd-doped YAG ceramics could replace YVO_4:Nd in such applications. This perspective changed when Taira et al. [6] discovered that the thermal conductivity of c-cut YVO_4 is higher than that of YAG. This breakthrough has since spurred the development of large-sized YVO_4 laser ceramics. However, fabricating a transparent YVO_4 ceramic is a big challenge because the birefringent scattering at the grain boundaries is large due to the non-cubic crystal structure causing the large refractive index anisotropy between its crystal axes. This scattering can lead to significant light losses and reduce the transparency and optical quality of the material. To minimize light scattering losses in non-cubic structured materials, controlling microstructures through grain size and textured structures is a promising approach

#538699 https://doi.org/10.1364/OE.538699
Journal © 2025 Received 16 Aug 2024; revised 28 Dec 2024; accepted 3 Jan 2025; published 9 Apr 2025

Optics EXPRESS

[7–12]. In addition to porosity, these microstructural factors have a significant impact on the optical properties of materials [13,14]. However, achieving smaller grain sizes often requires lower temperature processing, which can make it difficult to obtain pore-free dense bulks for optical applications.

The textured structure has recently attracted many attentions for the non-cubic crystal ceramic systems; the birefringent scattering at the grain boundaries can be reduced by aligning the crystal orientation of each grain. This method is particularly effective for non-cubic crystal ceramic systems because they exhibit birefringent scattering at the grain boundaries, which can negatively impact their optical properties. As a fabrication process of the textured ceramics, several approaches have been developed; for example, templated grain growth (TGG), [15] hot-forging [16] and magnetic field alignment methods [17,18]. Among them, the texture controlling through the magnetic field alignment technique is one of the most widely utilized methods not only for optical applications, but also for other fields of ceramic materials. Since template grain growth can be limited by the quality of the templates and the precise control over the alignment process. And the hot forging normally requires high temperatures and pressures that can introduce unwanted defects or stresses in the material, reducing the material quality. Whereas, the magnetic field alignment method is cost-effective, scalable, and easy to control over the above two methods. The principle of the magnetic field alignment process is as follows [19]. For the ceramics with anisotropic crystal structure, magnetic susceptibility is slightly different along different crystal axes. The strong magnetic field can align the crystal axis of ceramic particles dispersed in slurry and the strong texture can be developed during subsequent sintering [19–21]. For the YVO_4 particles with a tetragonal crystal structure, since the magnetic susceptibility should be different among the axes, if the strong magnetic field is applied to the YVO_4 slurry during slip casting processing, it is expected that the textured YVO_4 bulk materials can be synthesized after sintering to reduce the birefringent scattering loss at the grain boundaries.

For achieving the homogenous textured-microstructures, it is important to control the nanopowder slurry preparation to refrain from the agglomeration of fine particles. Colloidal technique is such a simple and cost-effective technique, which offers significant advantages to avoid agglomerates of fine particles by using electrostatic repulsive forces and/or steric stabilization. [7–10,22] During the colloidal processing, dispersant, solvent, pH adjustment and viscosity should be controlled. Among them, the dispersant will help to induce the electrostatic charge to enhance the stability of slurries through the electrostatic repulsion between particles. The suitable viscosity of the slurry, on the other hand, will help to keep kinetic stability by slowing down the particle aggregation and sedimentation which helps the particles having enough time to rotate under strong magnetic field, and finally, a homogeneous well-textured green body can be obtained under the strong magnetic field by using slip casting method via colloidal technique for slurry preparation.

In this work, therefore, the colloidal technique was utilized to prepare a YVO_4 nanopowder slurry with good dispersion and high stability. A magnetic field alignment technique was proposed, using the slip casting method, to fabricate a textured-YVO_4 green body. The green body was subsequently sintered using the SPS technique, which is a powerful sintering tool for achieving dense materials at relatively low temperatures to obtain the translucent YVO_4 ceramics.

2. Experimental procedure

2.1. YVO_4 nanopowders synthesis

The YVO_4 nanopowders were prepared using the same procedure as described elsewhere [23]. Briefly, NH_4VO_3 (Kanto Chemical Co., Japan, purity: analytical grade) was dissolved in a NaOH (Kanto Chemical Co., Japan, purity: > 99%) solution to produce a colorless solution with a concentration of 0.1 mol·L^{-1} (pH~12), during which VO_3^- was converted to VO_4^{3-}. This vanadate solution was then mixed with 2 mmol of $Na_2C_4H_4O_5$ (Kanto Chemical Co., Japan,

Optics EXPRESS

purity: > 99%), which was dissolved in 30 mL of an aqueous solution, followed by pH adjustment to ~12. Secondly, the resultant transparent solution was homogenized via magnetic stirring and then transferred to a stainless-steel autoclave for 30 h of hydrothermal reaction in an electric oven preheated to 200 °C. After the reaction, the hydrothermal YVO_4 nanopowders were collected via centrifugation, washed with water, and dried in air at 70 °C for 24 h.

2.2. Preparation of YVO_4 nanopowder slurry

The 15 vol% YVO_4 nanopowders were dispersed into distilled water with polyelectrolyte (poly(ammonium)acrylate A-6114, Toaghosei Co., Japan) as a dispersion media to obtain well dispersed YVO_4 slurry. The pH value of the YVO_4 slurries was adjusted to > 9 by Tetramethylammonium Hydroxide (TMAH). The adding amount of A-6114 was referred to 1wt% mass amount of YVO_4 in slurry. The slurry was then deagglomerated using a homogenizer for 10 minutes, followed by continuous stirring under ultrasonic dispersion for another 10 minutes.

2.3. Fabrication of textured-YVO_4 ceramic

The YVO_4 green body was fabricated from the slurry obtained as described above using slip casting in a strong magnetic field of $B = 12$ T by aligning the slip casting direction S parallel to the magnetic field B (Fig. 1). The resulting slip-cast YVO_4 green compacts were subjected to cold isostatic pressing (CIP) at 350 MPa for 10 min and were then densified in a graphite mold using a SPS machine (SPS, LABOX-315, Sinterland Co., Ltd., Japan) at the sintering temperatures of $T = 1100$-1300 °C with heating rates of 100 °C/min under a constant uniaxial pressure of 90 MPa. The pressure was increased to the target pressure of 90 MPa as the temperature rises from 1000 to 1100 °C. The temperature during sintering was monitored by measuring the temperature of hole on the mold using an optical pyrometer.

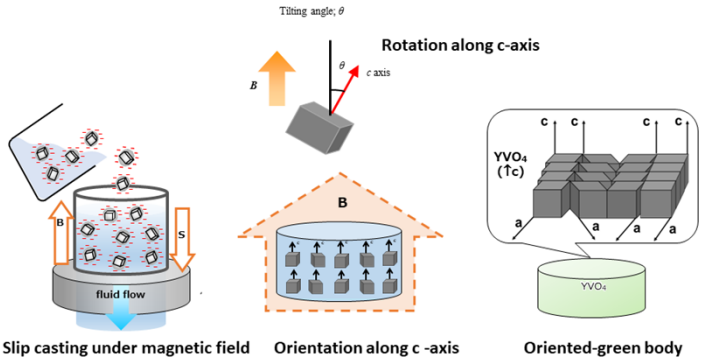

Fig. 1. Schematic illustrations of the preparation of (001) textured-YVO_4 green body with the slip casting direction S parallel to the magnetic field B during the slip casting under the strong magnetic field.

2.4. Characterization techniques

Slurry viscosities and Rheological behavior were measured as a function of the shear rate of the slurry by using a cone-plate viscometer (Re-215 Model, Toki Sangyo Co., Ltd., Tokyo, Japan). Zeta-potential measurement of the slurry was performed as a function of pH using zetasizer nano essentials (Malvern Instruments Ltd., United Kingdom). Particle size distribution was examined by a dynamic light scattering (DLS) analyzer (model Nanotrac UPA-UT 151, Nikkiso Co. Ltd., Tokyo, Japan).

X-ray diffraction (XRD) analysis of the YVO_4 nanopowders and sintered bodies were performed by RINT-TTR III diffractometer (Rigaku Co., Ltd, Tokyo, Japan, 40 kV 150 mA) using Cu Kα

Optics EXPRESS

radiation. Electron backscatter diffraction (EBSD, EDAX-TSL OIM EBSD system, EDAX Inc., USA) characterization was conducted for texture analysis, which was performed using a field-emission scanning electron microscope (JSM7000F, JEOL Ltd., Tokyo, Japan). Orientation Imaging Microscopy TM (TexSEM Laboratories, Inc., Draper, UT, United States of America) was used for collecting and analyzing the EBSD data. Microstructures of the nanopowders/ceramics were observed with a field emission scanning electron microscope (FE-SEM, JSM-7000, JEOL, Tokyo, Japan). Distribution of the grain size was calculated from EBSD data.

The transmittance in the wavelength range of $\lambda = 0.4\text{-}1.4\,\mu m$ were measured by using a double-beam spectrophotometer (SolidSpec-3700DUV, Shimadzu) equipped with an integrating sphere.

3. Results and discussion

3.1. Preparation and characterization of YVO_4 nanopowders and slurry

The XRD pattern of the nanopowders can only be indexed by tetragonal YVO_4 phase (Fig. 2(a)), and no any other impurity phases were identified. The morphology was further examined in detail using SEM, which revealed that the YVO_4 nanopowders exhibit a uniform morphology and excellent dispersion, as shown in Fig. 2(b). A narrow particle size distribution was achieved with a particle size of $d_{50} = 126\,nm$, according to the particle size distribution measurement in Fig. 2(c).

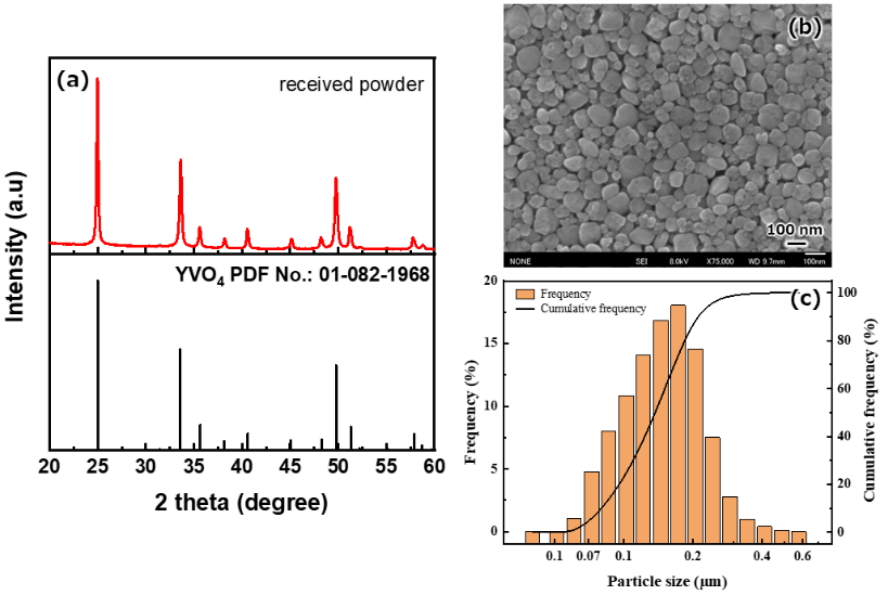

Fig. 2. XRD patterns (a), SEM image (b), and particle size distribution (c) of the YVO_4 nanopowders synthesized by using hydrothermal method.

The effect of pH on the zeta potential was considered for the YVO_4 slurry with the A6114 amount of 1wt%. As shown in Fig. 3(a), isoelectric point (pH_{IEP}) is about 5 for YVO_4 slurry. With increasing the pH value ($pH > pH_{IEP}$), the negative zeta potential increases accordingly. At the pH range of >9, the zeta potential value exceeds −40 mV, which is sufficient to prevent the particle aggregation by generating the repulsive force between the particles [24], indicating that the slurries with pH at this range (>9) can provide much better colloidal stability.

The rheological behavior, which evaluates powder dispersity in the slurries, was analyzed for the slurry containing 15 vol% YVO_4, 1 wt% of A6114 additive, and pH >9. The rheological

Optics EXPRESS

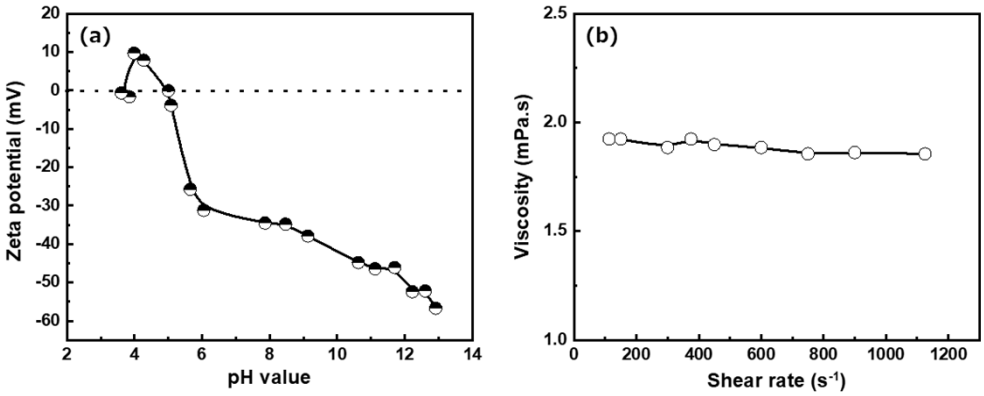

Fig. 3. (a) The effect of pH on the zeta potential of YVO_4 slurries with 1 wt% A6114, and (b) the shear rate dependence of the viscosities of the slurries with 15 vol% YVO_4.

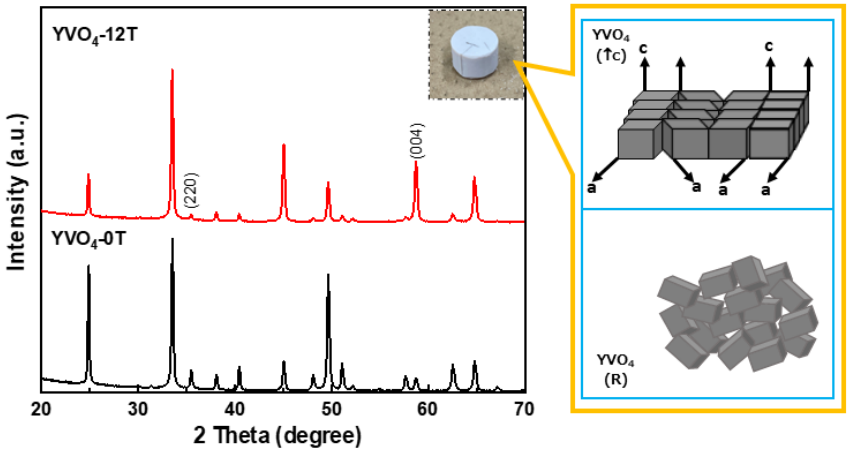

Fig. 4. XRD patterns of (001) textured-YVO_4 green body. For comparation, the XRD pattern of random YVO_4 green body is also presented.

behavior was assessed by measuring the effect of shear rate on the viscosity of the slurry. As shown in Fig. 3(b), the YVO_4 slurry exhibited relatively constant viscosities regardless of the shear rate, indicating a Newtonian response consistent with a well-dispersed powder slurry. The rheological measurements suggest that a well-dispersed and stable YVO_4 slurry can be obtained under the conditions investigated in this study.

3.2. *Characterization of crystalline orientation in YVO_4*

XRD patterns of YVO_4 green body, which was fabricated via slip casting in a strong magnetic field of $B = 12$ T with the slip casting direction S parallel to the magnetic field B are shown in Fig. 4. For comparison, the XRD pattern of random YVO_4 green body prepared outside of the magnet is also presented. The peak intensity ratio is slightly varies depending on the structure of YVO_4 prepared in a magnetic field. The reflection intensity of (004) plane at $2\theta = 58.64°$ is larger than that of the random YVO_4. The reflection intensities of (004) and (220) correspond to (001) plane and *a,b*-plane of YVO_4, respectively. Hence, the degree of (001) texture can be roughly estimated from the peak ratio P_{XRD} of the reflection intensities $I_{(004)}$ and $I_{(220)}$ of (004) and (220) planes, respectively. The P_{XRD} value is approximately 7.73 for textured-YVO_4 and

Optics EXPRESS

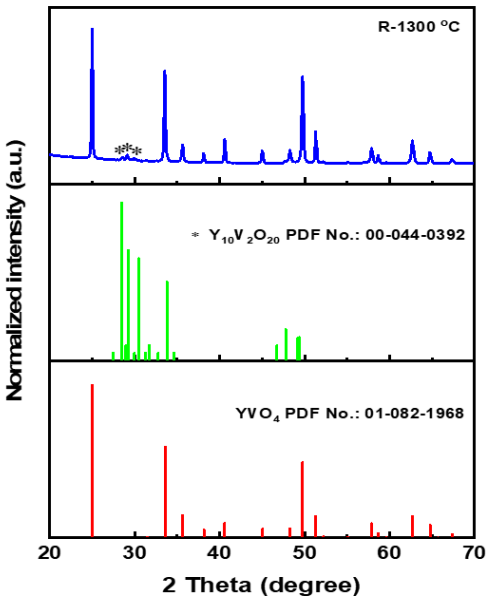

Fig. 5. XRD pattern of the random YVO_4 sintered at 1300 °C with a fixed dwelling time of 10 min and heating rate of 100 °C/min.

0.634 for the random sample, indicating that a well (001) textured-YVO_4 green body can be achieved under the strong magnetic field of $B = 12$ T. It was revealed that the c-axis was aligned parallel to the magnetic field and is easy magnetization axis.

The well-textured green bodies obtained above were then sintered by SPS under various temperatures with a fixed dwelling time of 10 min and heating rate of 100 °C/min, respectively. For comparison, the random YVO_4 sintered at 1300 °C with the same heating rate and dwelling time mentioned above is also fabricated. To accurately determine the impurity content in the sintered samples, XRD was only performed on random YVO_4 sample (Fig. 5), since the intensities of peaks (112), (103), and (004) with the tilting angle (θ) < 45° are enhanced in oriented samples, potentially affecting the precise determination of impurity content. The XRD reflection peaks in Fig. 5 are mainly indexed by the YVO_4 phase (PDF No.: 01-082-1968), and a small amount of $Y_{10}V_2O_{20}$-related peaks are detected in the sample, possibly due to the V-O evaporation during the sintering [25].

Texture structure of the SPSed samples were considered by SEM-EBSD for YVO_4 sintered under various temperatures. Figure 6 shows the EBSD inverse pole figure (IPF) map for the sample sintered at 1300 °C. The IPF map was colored against the vertical direction of the images, according to the color key on the standard stereographic triangle shown in Fig. 6. Most of the grains clearly show red and orange colors, indicating that the *c*-axis of most grains aligns perpendicular to the surface in the sample. This result demonstrates that by controlling the slip casting and the magnetic field set-up, the (001) textured structure can be successfully designed to align parallel to the YVO_4 surface.

The distributions of the tilt angle between the *c*-axis and the vertical direction in the YVO_4 sintered with various temperatures are calculated by using the multiples of a random distributions (MRD) from the EBSD data shown in Fig. 7(a). For comparation, MDR of random YVO_4 sintered with 1300 °C is also presented. For the random YVO_4, MDR is almost constant of ≈1 and no typical (001) orientation can be observed, whereas for the (001) textured samples, MRD shows a peak around $\theta = 0°$. The (001) planes of ~ 82%, ~86%, and ~91% grains are

Optics EXPRESS

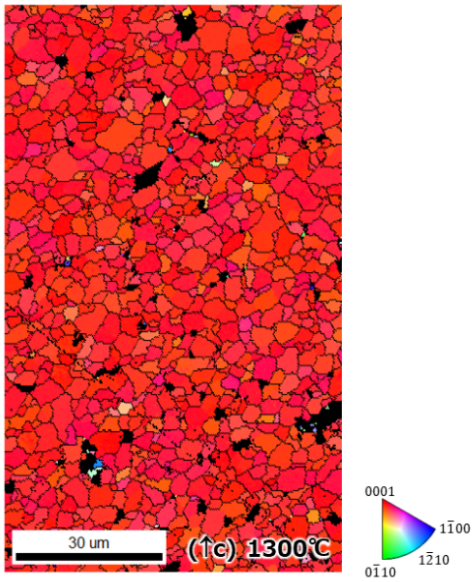

Fig. 6. EBSD inverse pole figure (IPF) mapping of the textured SPSed-YVO_4 sintered under 1300 °C.

aligned within the tilting range of $\theta = 0$-10° for textured YVO_4 fabricated with the temperatures of 1100 °C, 1200 °C, and 1300 °C, respectively. These results suggest that well-aligned (001) texture structure was obtained in textured YVO_4. Additionally, texture degree was enhanced with increasing sintering temperature from 1100 to 1300 °C for the samples fabricated from the textured green bodies. The development of texture degree with sintering temperature is generally attributed to grain coarsening [26]. According to Suzuki *et al.* [19], an increase in the texture degree due to the grain coarsening can be explained by the preferential growth of well-aligned larger grains over adjacent small grains with low orientation during sintering. The distribution of grain size which calculated from the EBSD data in Fig. 7(b) shows that the d_{50} increases from ~0.7 μm at $T = 1100$ °C to ~ 2.44 μm at $T = 1300$ °C. This result can be inferred that the initial well-aligned grain structure of the sample before sintering may contribute to the development of final texture at higher sintering temperatures.

Temperature dependent microstructures in Fig. 8 show that many residual pores are observed at multiple grain junctions at a lower temperature of $T = 1100$ °C and those apparently decrease with increasing the sintering temperature. For comparison, the microstructure of random YVO_4 ceramic sintered at 1300 °C is given in Fig. 8(d). Similar to the textured-YVO_4 sintered at the same sintering temperature, a few of residual pores can be observed at the multiple grain junctions as well (Fig. 8(c, d)), the grain size of random YVO_4 ceramic, however, is slightly larger than that of the textured-sample, with an average grain size of ~3.67 μm for the random sample compared to ~2.88 μm for the textured sample (Fig. 8(c, d)). This is because the grain boundary energy was influenced by the misorientation angle between adjacent grains. When the misorientation angle is large, as in the random sample, the grain boundary energy tends to be higher, which encourages grain coarsening. Whereas, in the oriented YVO_4 sample, the grains are aligned in a specific direction, which reduces the grain boundary misorientation angles between neighboring grains, leading to lower grain boundary energy and thus less grain coarsening. This can be demonstrated by the distribution of misorientation angles shown in Fig. 9. The misorientation angles in the random sample are much larger than those in the textured sample, indicating that many more high-angle boundaries can be observed in the random sample. Since grain boundaries

Optics EXPRESS

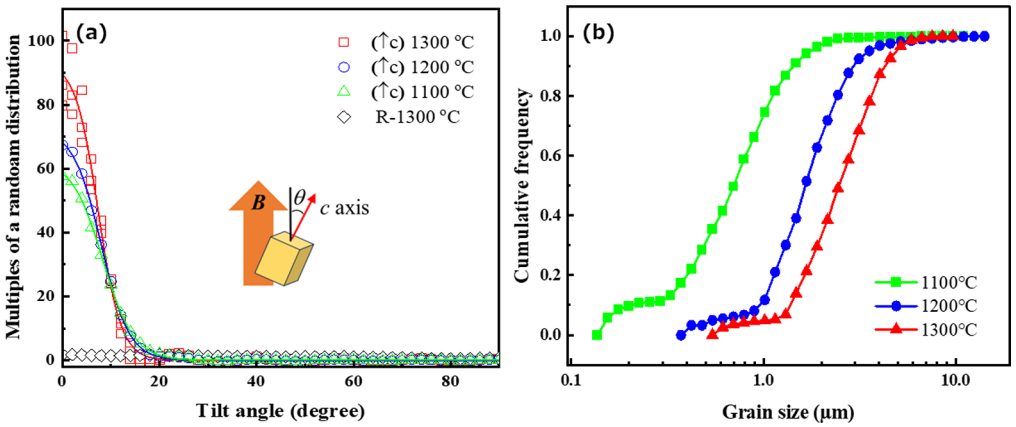

Fig. 7. (a) *c*-axis distribution, and (b) grain size distribution in the textured SPSed-YVO_4 sintered under various temperatures, which is calculated from the EBSD data.

act as barriers to grain growth, these higher energy grain boundaries are less effective barriers, ultimately leading to a larger grain size in the random sample. Additionally, the misorientation angle distribution curve for the random sample is very similar to the Mackenzie ideal line, which is normally used to represent the theoretical distribution of grain boundary misorientation angles for an ideal random texture in polycrystalline materials [27]. Whereas a significant deviation can be observed between the misorientation distribution of textured sample and Mackenzie distribution, further confirming that textured structure was successfully designed in the sample prepared under the magnetic field.

3.3. *Optical properties of (001) textured-YVO_4 ceramics*

Figure 10 gives the transmittance efficiencies of both textured- and random YVO_4 sintered at 1300 °C in the wavelength range from the visible to near-IR wavelength of $\lambda = 0.4$ -1.4 μm. The uneven profile around the wavelength of 900 nm is due to the equipment and does not reflect the properties of the sample. The transmittance is sensitive to textured structure of YVO_4, which exhibits much higher transmittance value than that of the random sample for the same sintering conditions at the whole measurement wavelength range. For the YVO_4 with non-cubic structure, the transmittance is known to be highly sensitive to all the microstructural factors of texture, grain size and porosity. Compared to the random YVO_4 sample, YVO_4 with (001) orientation can improve the transmittance by reducing the birefringence at the grain boundary through development of (001) texture in YVO_4. The transmittance, however, is not determined only by one microstructural factor of the (001) texture, but also affected by other microstructural factors of the grain size and porosity [28,29]. Both samples exhibit the similar porosity, as shown in Fig. 8(c), (d), the larger grain size, however, in the random YVO_4 sample (3.67 μm) would increase the birefringent scattering loss at the grain boundaries, and may thus also cause the reduction in transmittance of the random sample. These results suggest that the (001) textured structure of YVO_4 ceramics, is sufficiently effective in suppressing the birefringent scattering at the grain boundaries, and hence, effectively contributed to enhance the transmittance of YVO_4.

Optics EXPRESS

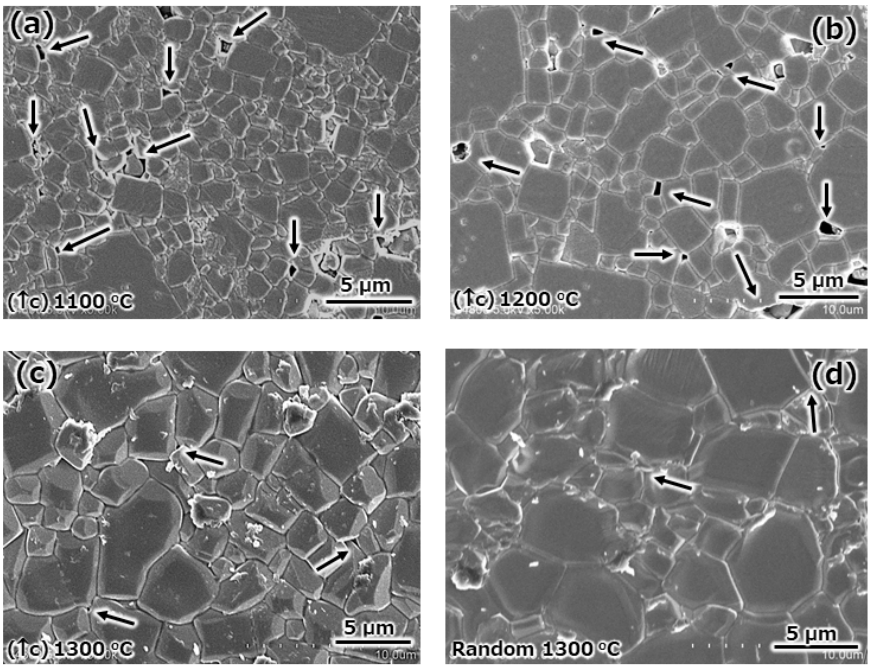

Fig. 8. SEM images of (001) textured-YVO_4 ceramics fabricated at (a) 1100 °C, (b) 1200 °C, (c) 1300 °C, and (d) the SEM image of random YVO_4 fabricated at 1300 °C, with a constant dwelling time of 10 min and a heating rate of 100 °C/min.

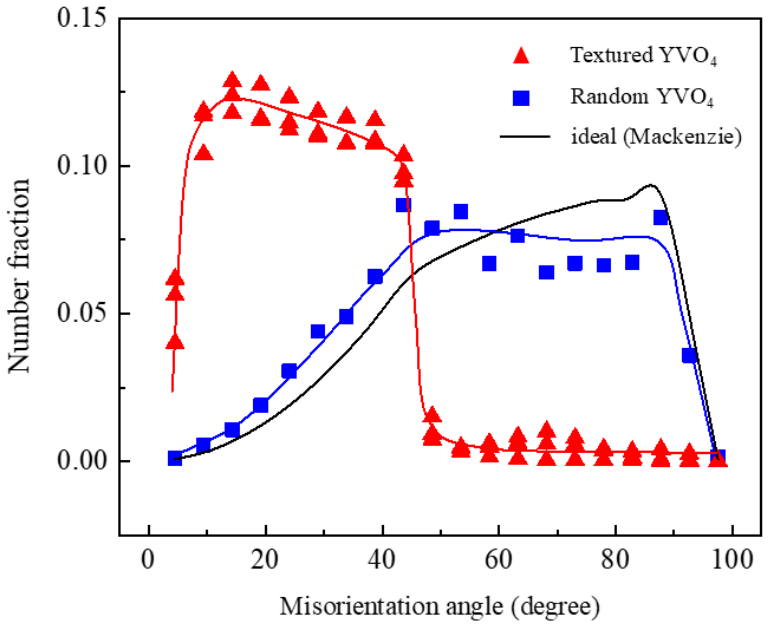

Fig. 9. Distribution of misorientation angle in random and textured YVO_4. The ideal line of MacKenzie is also presented.

Optics EXPRESS

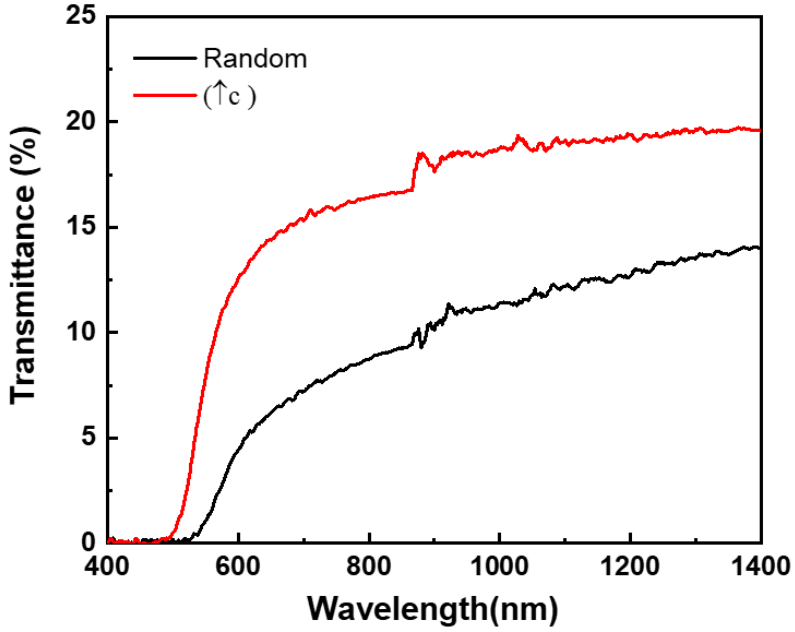

Fig. 10. Transmittance efficiencies of the (001) textured- and the random YVO_4 ceramics fabricated at 1300 °C with a constant dwelling time of 10 min and a heating rate of 100 °C/min.

4. Conclusions

A well-dispersed and highly stable slurry with 15 vol% YVO_4 was achieved by a colloidal technique using 1 wt% A6114 as dispersant at the slurry pH > 9. The (001) textured YVO_4 was successfully formed by controlling the crystalline orientation through the strong magnetic field alignment processing during the slip casting. As the SPS sintering temperature increased from 1100 to 1300 °C, grain size and density increased, and the orientation of the sample improved as well. For the optimum SPS processing at $T = 1300$ °C for dwelling time of 10 min and heating rate of 100 °C /min, the (001) textured-YVO_4 exhibits much higher transmission efficiency at the whole wavelength range than that of the non-textured random YVO_4 sample, indicating that controlling the microstructure using a textured structure method is a suitable way to enhance the transmittance of YVO_4 ceramics. It is expected that this method can be easily applied and orientation can be achieved even when Nd is doped into YVO_4.

Funding. Innovative Science and Technology Initiative for Security (JPJ004596).

Acknowledgments. Part of this work was financially supported by Innovative Science and Technology Initiative for Security, Grant Number JPJ004596, ATLA, Japan.

Disclosures. The authors declare no conflicts of interest.

Data availability. Data underlying the results presented in this paper are not publicly available at this time but may be obtained from the authors upon reasonable request.

References

1. B. L. Davydov, "Single-prism polarizer for laser emission with higher power," J. Opt. Technol. **89**(6), 332–338 (2022).
2. S. Huang, Z. Fan, Q. Zhu, *et al.*, "Coordination polymer templated engineering of YVO_4 : Eu submicron crystals and photoluminescence," CrystEngComm. **22**(6), 1024–1031 (2020).
3. R. A. Fields, M. Birnbaum, and C. L. Fincher, "Highly efficient Nd: YVO_4 diode-laser end-pumped laser," Appl. Phys. Lett. **51**(23), 1885–1886 (1987).

Optics EXPRESS

4. T. Taira, A. Mukai, Y. Nozawa, *et al.*, "Single-mode oscillation of laser-diode-pumped Nd : YVO_4 microchip lasers," Opt. Lett. **16**(24), 1955–1957 (1991).
5. I. Shoji, S. Kurimura, Y. Sato, *et al.*, "Optical properties and laser characteristics of highly Nd^{3+}-doped $Y_3Al_5O_{12}$ ceramics," Appl. Phys. Lett. **77**(7), 939–941 (2000).
6. Y. Sato and T. Taira, "The studies of thermal conductivity in $GdVO_4$, YVO_4, and $Y_3Al_5O_{12}$ measured by quasi-one-dimensional flash method," Opt. Express **14**(22), 10528–10536 (2006).
7. T. Carisey, I. Levin, and D. G. Brandon, "Microstructure and mechanical properties of textured Al_2O_3," J. Eur. Ceram. Soc. **15**(4), 283–289 (1995).
8. F. V. DiMarcello, P. L. Key, and J. C. Williams, "Preferred orientation in Al_2O_3 substrates," J. Am. Ceram. Soc. **55**(10), 509–514 (1972).
9. T. S. Suzuki, T. Uchikoshi, H. Okyama, *et al.*, "Mechanical properties of textured, multilayered alumina produced using electrophoretic deposition in a strong magnetic field," J. Eur. Ceram. Soc. **26**(4-5), 661–665 (2006).
10. T. S. Suzuki, T. Uchikoshi, and Y. Sakka, "Control of texture in alumina by colloidal processing in a strong magnetic field," Sci. Technol. Adv. Mat. **7**(4), 356–364 (2006).
11. Y. Ma and K. J. Brownman, "Texture in Hot-Pressed or Forged Alumina," J. Am. Ceram. Soc. **74**(11), 2941–2944 (1991).
12. E. Suvaci and G. L. Messing, "Critical factors in the templated grain growth of textured reaction-bonded alumina," J. Am. Ceram. Soc. **83**(8), 2041–2048 (2000).
13. L. H. Liu, K. Morita, T. S. Suzuki, *et al.*, "Effect of volume ratio on optical and mechanical properties of Y_2O_3-MgO composites fabricated by spark-plasma-sintering process," J. Eur. Ceram. Soc. **41**(3), 2096–2105 (2021).
14. L. H. Liu, K. Morita, T. S. Suzuki, *et al.*, "Evolution of microstructure, mechanical, and optical properties of Y_2O_3-MgO nanocomposites fabricated by high pressure spark plasma sintering," J. Eur. Ceram. Soc. **40**(13), 4547–4555 (2020).
15. Q. Yang, H. Wang, S. Chen, *et al.*, "Highly-oriented (104) polycrystalline α-Al_2O_3 transparent ceramics prepared by a templated grain growth method," J. Eur. Ceram. Soc. **39**(4), 1721–1724 (2019).
16. Y. Yoshizawa, M. Toriyama, and S. Kanzaki, "Fabrication of Textured Alumina by High-Temperature Deformation," J. Am. Ceram. Soc. **84**(6), 1392–1394 (2001).
17. X. Mao, S. Wang, S. Shimai, *et al.*, "Transparent polycrystalline alumina ceramics with orientated optical axes," J. Am. Ceram. Soc. **91**(10), 3431–3433 (2008).
18. T. S. Suzuki, Y. Sakka, and K. Kitazawa, "Orientation amplification of alumina by colloidal filtration in a strong magnetic field and sintering," Adv. Eng. Mater. **3**(7), 490–492 (2001).
19. T. S. Suzuki, "Advanced control of crystallographic orientation in ceramics by strong magnetic field," J. Ceram. Soc. Jpn. **128**(12), 1005–1012 (2020).
20. T. Ashikaga, B. N. Kim, H. Kiyono, *et al.*, "Effect of crystallographic orientation on transparency of alumina prepared using magnetic alignment and SPS," J. Eur. Ceram. Soc. **38**(7), 2735–2741 (2018).
21. T. S. Suzuki, T. Uchikoshi, and Y. Sakka, "Effect of sintering additive on crystallographic orientation in AlN prepared by slip casting in a strong magnetic field," J. Eur. Ceram. Soc. **29**(12), 2627–2633 (2009).
22. C. Zhang, T. Uchikoshi, L. H. Liu, *et al.*, "Synthesis of Eu-doped hydroxyapatite whiskers and fabrication of phosphor layer via electrophoretic deposition process," J. Am. Ceram. Soc. **103**(12), 6780–6792 (2020).
23. S. Huang, X. Wang, Q. Zhu, *et al.*, "Systematic synthesis of $REVO_4$ micro/nano crystals with selective exposure of high energy {001} facets and luminescence (RE = Lanthanide and $Y_{0.95}Eu_{0.05}$)," J. Mater. Res. Technol. **9**(6), 12547–12558 (2020).
24. J. Duffy, A. Hill, A. Walton, *et al.*, "Slurry Stability: Why Particle Size, Zeta Potential and Rheology are Important," Ann. T. Nord. Rheol. Soc. **20**, 209–214 (2012).
25. S. Erdei, G. G. J. R. Johnson, and F. W. Ainger, "Growth studies of YVO_4 crystals (II). Changes in Y-V-O-stoichiometry," Cryst. Res. Technol. **29**(6), 815–828 (1994).
26. E. Guilmeau, D. Chateigner, T. S. Suzuki, *et al.*, "Rietveld texture analysis of alumina ceramics by neutron diffraction," Chem. Mater. **17**(1), 102–106 (2005).
27. J. K. Mackenzie, "Second paper on statistics associated with the random disorientation of cubes," Biometrika **45**(1-2), 229–240 (1958).
28. H. Shahbazi, M. Tataei, M. H. Enayati, *et al.*, "Structure-transmittance relationship in transparent ceramics," J. Alloys Compd. **785**, 260–285 (2019).
29. B. N. Kim, K. Hiraga, K. Morita, *et al.*, "Spark plasma sintering of transparent alumina," Scripta Mater. **57**(7), 607–610 (2007).